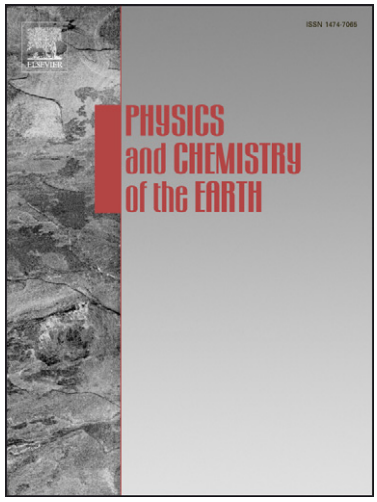

Modeling the influence of $MgSO_4$ invariant points on multiphase reactive transport process during saline soil evaporation

P. Gamazo, M.W. Saaltink, J. Carrera, L. Slooten, S.A. Bea, M. Gran

PII: S1474-7065(13)00005-3
DOI: http://dx.doi.org/10.1016/j.pce.2013.02.001
Reference: JPCE 2172

To appear in: *Physics and Chemistry of the Earth*

Please cite this article as: Gamazo, P., Saaltink, M.W., Carrera, J., Slooten, L., Bea, S.A., Gran, M., Modeling the influence of $MgSO_4$ invariant points on multiphase reactive transport process during saline soil evaporation, *Physics and Chemistry of the Earth* (2013), doi: http://dx.doi.org/10.1016/j.pce.2013.02.001

Modeling the influence of $MgSO_4$ invariant points on multiphase reactive transport process during saline soil evaporation.

P. Gamazo[a,b], M.W. Saaltink[b], J. Carrera[c], L. Slooten[c], S.A. Bea[d] and M. Gran[b]

a Departamento del Agua, Regional Norte, Universidad de la República, Gral. Rivera 1350, 50000 Salto, Uruguay

b GHS, Dept Geotechnical Engineering and Geosciences, Universitat Politecnica de Catalunya, UPC-BarcelonaTech, c/Jordi Girona 1-3, 08034 Barcelona, Spain

c GHS, Institute of Environmental Assessment and Water Research (IDAEA), CSIC, c/Lluis Solè Sabarìs, s/n, 08028 Barcelona, Spain

d CONICET-IHLLA-UNICEN República de Italia 780, Azul, Buenos Aires, C.C. 47 (B7300) Argentina

Abstract:

In the present work, we modeled a laboratory experiment where a sand column saturated with a $MgSO_4$ solution is subject to evaporation. We used a compositional formulation capable of representing the effect of geochemistry on flow and transport for concentrated solutions under extreme dry conditions. The model accounts for the water sink/sources terms due to hydrated mineral dissolution/precipitation and the occurrence of invariant points, which prescribe the water activity. Results show that the occurrence of the invariant points at the top of the domain could affect the vapor flux at the column top and salt precipitation along the column. In fact, the invariant points occurrence could explain the spatial fluctuation on the salt precipitates formation. Results also suggest that the complex hydrochemical interactions occurring during soil salinization, including osmotic effects, are crucial not only to understand the salt precipitation, but also the evaporation rate.

Keywords:

- soil evaporation
- hydrated minerals
- invariant point
- coupling effects
- multiphase reactive transport

Highlights:

- Modeling evaporation of sand column with $MgSO_4$ solution.
- Model involves oven dry conditions, high salinity, hydrated mineral precipitation.
- Coupling effects: geochemical reactions on water content and therefore on flow.

- Modeling invariant points: mineral paragenesis prescribes water activity.
- Invariant points affects evaporation, vapor flux, salt distribution

1. Introduction

Evaporation in soils is an important component of the hydrological cycle because it exerts a significant influence on soil water budget. Evaporation triggers a series of complex processes, like liquid and gaseous mass flow, energy flow, solute reactive transport and eventually salt precipitation. Numerical modeling of these processes, in combination with field and laboratory experiments, provides the means for testing conceptual models and for evaluating complex interactions of processes in soils and other porous media (Steefel et al. 2005). Models allow obtaining quantitative approximations of processes and variables that are difficult or impossible to measure directly in field or laboratory.

Unsaturated liquid water flow was the first process modeled in soil evaporation codes (Remson et al., 1971). Since then, more complex processes have been added to soil evaporation models including vapor flux (Fayer et al. 1986), interaction between water and heat flow (Milly 1980), and salinity effects on evaporation (Nassar and Horton 1989). More recently, the modeling of soil salinization, biological nutrient degradation and evolution of mine tailings have led to the inclusion of reactive transport in soil evaporation modeling (Zee, 1990). Wissmeier and Barry (2008) compiled several examples in agricultural and environmental engineering, including water irrigation efficiency (Wenninger et al. 2010), water management practices and irrigation techniques in arid and semiarid areas (Cortes-Jimenez et al., 2007: Xu et al. 2002), reclamation strategies for sodic soils (Bauer et al. 2006, Qadir et al. 2000) , evaluation of the suitability of irrigation waters (Ghassemi et al. 1991), and acid mine drainage and rehabilitation of residue disposal sites (Acero et al., ; 2009; Bea et al., 2010b., Lefebvre, 2001; Mayer et al., 2006). Numerical modeling has also been used for designing and analyzing evaporation experiments and has helped to improve the understanding of salt and efflorecense precipitation and evaporation at the macro and pore scales in homogeneous and heterogeneous porous media (Bechtold et al. 2011, Guglielmini et al. 2008, Nachshon et al. 2011, Rad and Shokri 2012).

One aspect that has not been considered, even in the most advanced codes, is the effect of geochemical reactions on water content and thus on flow (Wissmeier and Barry 2008). This reflects the fact that geochemical effects on water balance can be neglected in most cases.

However, in arid or semiarid climates soils may reach extremely dry conditions, so that hydrated mineral dissolution/precipitation may generate water sinks/source terms comparable to the remaining processes. Another potentially relevant often ignored aspect in saline and dry conditions, is the occurrence of invariant points. In such cases, mineral paragenesis (typically, simultaneous presence of several minerals with similar stoichiometry but different levels of hydration) prescribes water activity (Bea et al., 2010a; Gamazo et al., 2011; Risacher and Clement, 2001). Vapor partial pressure, which controls evaporation rate, depends on water activity (Dao et al., 2008). Therefore, at invariant points, mineral phases are controlling the evaporation rate by fixing vapor pressure.

Gran et al. (2011a) conducted an experiment in which the occurrence of invariant points is expected. In this experiment a sand column, initially saturated with a MgSO4 solution, was subject to a constant source of heat at the top. During the experiment, extreme dry conditions were reached and magnesium sulphate started to precipitate. These precipitates are highly hygroscopic and produce different mineral phases depending on their degree of hydration. The quantification of these minerals is not easy, since they may modify its hydration water content during handling or X-ray irradiation (García-Guinea et al., 2000). In this case numerical modeling, combined with observations, may be useful for evaluating the occurrence of invariant points and their influence on hydrodynamic processes. Gran et al. (2011b) modeled this experiment but by decoupling flow from reactive transport calculations and not considering invariant points.

The aim of this paper is to study the interaction of hydrated mineral precipitation and hydrodynamic processes on Gran's experiment using PROOST (Slooten et al., 2010) a new multi-phase reactive transport code capable of modeling multiphase reactive transport of concentrated solutions under dry conditions. PROOST considers a compositional formulation that allows representing invariant points and the influence of geochemical source sink terms on phase flows (Gamazo et al.,2012). Therefore it can be used to estimate the influence of these factors on the hydrodynamic processes of the experiment.

2. Model description

2.1. Conceptual model

The column experiment is described in detail in Gran et al. (2011a). A 24 cm and 14.4 cm in diameter silica sand column (0.4–0.8 mm grain size and 2.65 g/cm^3 density), initially saturated with a $MgSO_4$ solution, was subject to a constant source of heat on the upper part. The column

was isolated except at the top, allowing free vapor exchange with the laboratory atmosphere. The incoming heat produces water evaporation which reduces the saturation degree at the top of the column and induces an upward unsaturated liquid flow. The liquid flow transports solutes which results in an increase of concentrations in the evaporation zone and eventually salt precipitation. Evaporation is then affected by osmotic effects due to high solute concentrations and by capillarity effects due to low saturations degrees. The reduction of the evaporation rate and hydraulic conductivity at the upper part of the column produces a descending evaporation front that affects both vapor and energy fluxes. The processes and interactions mentioned show the high degree of coupling between the various phenomena of the problem.

2.2 Processes and governing equations

2.2.1 Global equations: mass and energy conservation principles

Most multiphase reactive transport codes decouple phase conservation, or major component conservation, from reactive transport equations (TOUGHREACT, Xu and Pruess, 1998; CODEBRIGHT-RETRASO, Saaltink et al., 2004; MUFTE-UG, Ebigbo et al., 2006; MIN3P Molins and Mayer, 2007; PFLOTRAN, Mills et al., 2007). Therefore, they solve first fluid phases balances, and optionally energy transport, and secondly component conservation equations. For this work we considered the compositional formulation presented in Gamazo et al. (2012), in which no explicit phase conservation is considered. This is possible because the formulation considers the fact that a phase conservation equation is equal to the sum of the conservation of all species that comprise it.

The component mass conservation equations can be written using a vector notation as:

$$\frac{\partial}{\partial t}\left(\theta_{aq}\mathbf{u}_{aq}\right)+\frac{\partial}{\partial t}\left(\theta_{g}\mathbf{u}_{g}\right)+\frac{\partial}{\partial t}\left(\mathbf{u}_{imm}\right)=\mathbf{L}_{aq}\left(\mathbf{u}_{aq}\right)+\mathbf{L}_{g}\left(\mathbf{u}_{g}\right)+\mathbf{f}^{'} \tag{1}$$

where θ_{aq} and θ_{g} are the volumetric content of aqueous and gaseous phase, $\mathbf{u}_{aq}$, $\mathbf{u}_{g}$, $\mathbf{u}_{imm}$ are the aqueous, gaseous and immobile portions of the components vectors, $\mathbf{L}_{aq}(\ )$ and $\mathbf{L}_{g}(\ )$ are the aqueous and gaseous transport operators, and $\mathbf{f}^{'}$ is the vector of source-sink terms.

The different portions of the components vectors are defined as:

$$\mathbf{u}_{aq} = \mathbf{U} \cdot \begin{pmatrix} \mathbf{c}_{aq} \\ 0 \\ 0 \end{pmatrix}; \mathbf{u}_{g} = \mathbf{U} \cdot \begin{pmatrix} 0 \\ \mathbf{c}_{gas} \\ 0 \end{pmatrix}; \mathbf{u}_{imm} = \mathbf{U} \cdot \begin{pmatrix} 0 \\ 0 \\ \mathbf{c}_{imm} \end{pmatrix} \quad (2)$$

were $\mathbf{c}_{aq}$, $\mathbf{c}_{gas}$, $\mathbf{c}_{imm}$ are vectors with the aqueous, gaseous and immobile species concentrations, and $\mathbf{U}$ is the component matrix. Details on the calculation of $\mathbf{U}$ are given in Saaltink et al. (1998) and Gamazo et al. (2012).

The transport operator of the mobile phase α (aq or gas) includes advection and diffusion-dispersion $L_\alpha\left(u_{i,\alpha}\right) = -\nabla\cdot\left(u_{i,\alpha}\mathbf{q}_\alpha\right) - \nabla\cdot\left(\mathbf{j}_{D_\alpha,i}\right)$. Mobile phase fluxes $\mathbf{q}_\alpha$ are calculated according to Darcy's law: $\mathbf{q}_\alpha = -\frac{\mathbf{K}k_{r,\alpha}}{\mu_\alpha}\left(\nabla p_\alpha - \rho_\alpha \mathbf{g}\right)$, were $\mathbf{K}$ is the intrinsic permeability, $k_{r,\alpha}$ is the relative phase permeability, μ_α, p_α and ρ_α are the viscosity, pressure, and density of the α phase, and $\mathbf{g}$ is the gravity vector. Diffusive-dispersive fluxes $\mathbf{j}_{D_\alpha,i}$ are calculated according to Fick's law: $\mathbf{j}_{D_\alpha,i} = -\left(\mathbf{D}_\alpha^{diff}\phi\theta_\alpha\tau + \mathbf{D}_\alpha^{disp}\right)\cdot\nabla\left(u_{i,\alpha}\right)$, where $\mathbf{D}_\alpha^{diff}$ is the diffusive phase tensor, ϕ is the porosity, τ is the tortuosity and $\mathbf{D}_\alpha^{disp}$ is the phase dispersion tensor (See Table 1).

The external source-sink term is defined as $\mathbf{f}' = \mathbf{U}\cdot\mathbf{f}$, where $\mathbf{f}$ is the vector of source-sink terms for each species.

By assuming thermal equilibrium among phases, an unique energy conservation equation is considered:

$$\sum_\alpha \frac{\partial}{\partial t}\left(\theta_\alpha E_\alpha\right) = -\nabla\left(\mathbf{i}_c\right) - \sum_\alpha \nabla\left(\mathbf{i}_{E,\alpha}\right) + f_E \quad (3)$$

where E_α is the volumetric internal energy of phase α, $\mathbf{i}_c$ is the conductive heat flux, $\mathbf{i}_{E,\alpha}$ is the heat flux due to phase α motion, and f_E is a sink-source term.

The volumetric internal energy of phase α is calculated as $E_\alpha = \sum_{i=1}^{N_{s,\alpha}} c_{i,\alpha} e_{i,\alpha}$, where $e_{i,\alpha}$ is the molar internal energy of the specie i in phase α. The conductive heat flux is calculated according to Fourier's law $\mathbf{i}_c = -k_c^T\left(\nabla T\right)$, where k_c^T is the thermal conductivity of the medium and T is temperature. The heat flux due to the motion of phase α is calculated from

$\mathbf{i}_{E,\alpha} = \mathbf{q}_\alpha E_\alpha - \left(\mathbf{D}_\alpha^{diff}\phi\theta_\alpha\tau + \mathbf{D}^{disp}\right)\cdot \nabla E_\alpha$. For this application energy balance was reduced to enthalpy balance. Therefore, pneumatic effects were not considered.

2.2.2 Local equations: constitutive and thermodynamic expressions

Problem parameters and constitutive models used are shown in Table 1. As extreme dry conditions are reached, we consider a retention curve capable of representing oven dry conditions (Fayer and Simmons, 1995, Massana, 2005; Silva and Grifoll, 2007, Gran et al. 2011b). The modified van Genuchten retention curve considers a variable minimum degree of saturation

$$S_i = S_{\min}^0 \beta \ln\left(P_c^{dry} \Big/ \left(P_g - P_{aq}\right)\right) \tag{4}$$

where $S_{\min}^0$ is the residual saturation for which liquid water becomes discontinuous and, hence, liquid permeability becomes zero, P_c^{dry} is the capillary pressure for the dry material and β is a parameter that scales the transition from the standard to the oven dry branch of the curve. For the liquid relative permeability function, we consider an effective saturation

$$S_e^{'} = \left(S_{aq} - S_{\min}^0\right) \Big/ \left(1 - S_{\min}^0\right) \tag{5}$$

and a smooth transition for the relative permeability $K_{r,aq}$ from $K_{r,aq}^0$ to zero, when saturation varies between $S_{aq,min}$ and $S_{\min}^0$

$$K_{r,aq} = \begin{array}{ll} K_{r,aq}^0 & S_{aq} > S_{aq,min} \\ K_{r,aq}^0 \left(S_{aq} / S_{aq,min}\right)^\gamma & S_{aq} < S_{aq,min} \end{array} \tag{6}$$

where $K_{rl,aq}^0$ is the standard van Genuchten permeability and γ is a smoothing parameter.

A single molecular diffusion coefficient was used for all species on each phase and enhancement in vapor diffusion was considered by assuming $\theta_{gas}\tau$ equal to one for the gaseous phase.

In this experiment high concentrations are produced in low saturations zones where liquid relative permeability is reduced in several orders of magnitude or where liquid water has become discontinuous and relative permeability is zero. Viscosity can be affected by salinity, but its value can raise up to 6 times fresh water value for concentrated solutions with a mass

fraction of 0.6 depending on brine composition (Kwak et al. 2005, Lide 2000). Therefore, salinity effects can be discounted from liquid viscosity for this model.

We consider the same parameters as Gran et al. (2011b) with the exception of gas diffusion and thermal conductivity. The model Gran et al. (2011b) defines two zones for these parameters: the upper 1.5 cm of the column with a reduced diffusion coefficient and a higher thermal conductivity, and the rest of the column. This zonation was made in order to reproduce changes on these properties due to mineral precipitation in the upper part of the column. In our model we define homogeneous properties on the column.

Table 1 - Constitutive equations

2.2.3 Geochemistry

Due to the high ionic strength the values of the thermodynamic activity coefficients were computed using the Pitzer (1973) ion–ion interaction model with the parameters given by Harvie et al. (1984). The chemical reactions considered in the simulation are summarized in Table 2.

Table 2 – Chemical reactions considered

The psychrometric law was used to calculate the capillary effect on water activity:

$$f_{cap} = \exp\left(\frac{\left(p_g - p_{aq}\right)\cdot M_{H_2O}}{RT\,\rho_{aq}}\right) \tag{7}$$

where p_g and p_{aq} are the gaseous and liquid pressure, M_{H_2O} is molar weight of water, R is the universal gas constant and ρ_{aq} is liquid density. Thus, the water activity is $a_{H_2O} = f_{cap}\cdot a_{H_2O}^{osmotic}$, where $a_{H_2O}^{osmotic}$ is the activity of liquid water given by the Pitzer ion interaction model. Equation (7) illustrates the importance of water activity to link geochemical and hydrodynamic processes.

When rich $MgSO_4$ water evaporates a sequence of hydrated $MgSO_4$ minerals is expected to precipitate: epsomite ($MgSO_4\cdot 7H_2O$), hexahydrite ($MgSO_4\cdot 6H_2O$) and kieserite

($MgSO_4 \cdot H_2O$). Within the ranges of temperature and relative humidity of the experiment these are the only stable magnesium sulfates minerals. Starkeyite ($MgSO_4 \cdot 4H_2O$) is metastable for low relative humidity values, and pentahydrite ($MgSO_4 \cdot 5H_2O$) and sanderite ($MgSO_4 \cdot 2H_2O$) are unstable (Grevel and Majzlan 2009, Wang et al. 2009).

Magnesium sulfate minerals, like other hydrated minerals and efflorescent salts (e.g. gypsum, bischofite, bloedite, kainite) can act as a water source or sink as they dissolve or precipitate, and certain combinations of these minerals can literally control water activity (Bea et al., 2010a; Gamazo et al., 2011; Risacher and Clement, 2001). This can be illustrated by considering the coexistence in equilibrium of epsomite and hexahydrite. Expressing the mass action law for both minerals yields water activity as:

$$\begin{aligned} a_{Mg^{2+}} a_{SO_4^{2-}} a_{H_2O}^7 &= K_{epsomite} \\ a_{Mg^{2+}} a_{SO_4^{2-}} a_{H_2O}^6 &= K_{hexahydrite} \end{aligned} \quad \Rightarrow a_{H_2O} = \frac{K_{epsomite}}{K_{hexahydrite}} \tag{8}$$

Water activity will be fixed by the water sink-source term that results from combining epsomite dehydration and hexahydrite precipitation:

$$epsomite \Leftrightarrow hexahydrite + H_2O \tag{9}$$

This water sink-source affects the liquid mass balance and it may be relevant for in case of very low water content scenarios. As water activities is calculated considering osmotic effects (Pitzer model) and capillary effects (Psychometric law), invariant points not only affect geochemical variables but also vapor pressure. Therefore, a fully coupled solution of phase fluxes and reactive transport is necessary.

There are several mineral combinations that can fix water activity, like hexahydrite and kieserite ($a_{H_2O} = \left(K_{hexahydrite} / K_{kieserite}\right)^{1/5}$), gypsum and anhydrite ($a_{H_2O} = \sqrt{K_{gypsum} / K_{anhydrite}}$) or more complex combinations like gypsum, mirabilite and glaberite ($a_{H_2O} = \left(K_{gypsum} \cdot K_{mirabilite} / K_{glauberite}\right)^{1/12}$) (Bea et al., 2010a; Gamazo et al., 2011; Risacher and Clement 2001).

Precipitation rate data do not exist for most minerals (Palandri and Kharaka 2004), and literature about magnesium sulfate kinetics is scarce (Al-Jibbouri et al. 2002. Sgualdino et al.

1987). Most geochemical codes consider evaporite mineral precipitation/dilution in equilibrium (PHREEQC, Parkhurst and Appelo, 1999, EQL/EVP, Risacher and Clement, 2001). For the simulation of this experiment we consider all mineral magnesium sulfate in equilibrium.

2.3 Numerical model

The code PROOST was used to carry out the numerical simulation (Slooten et al., 2010). PROOST is a general purpose hydrological modeling tool that can solve a large variety of conservation equations expressed as partial differential equations. It was programed following the object oriented (OO) paradigm in FORTRAN 95. All geochemical processes where included in PROOST by adding CHEPROO (Bea et al., 2009) to its framework. CHEPROO is an OO tool specialized in complex geochemical processes.

The experiment was modeled considering a 1D domain. The column was assumed to be initially saturated and at a temperature of 25°C. Boundary conditions at the top of the domain include vapor exchange with the laboratory atmosphere due to advective and diffusive fluxes, and an incoming flux of energy. The rest of the domain had no mass exchange and a linear heat loss. Boundary and initial conditions details are given in Table 3.

The problem was solved using the Direct Substitution Approach (DSA, see Saaltink et al., 1998 and Gamazo et al., 2012 for details) and the finite element method was used to solve the partial differential equations. Node spacing was set to 0.2 mm for the upper 2 cm of the column, 1mm for the following 6 cm, and 8mm for the final 16 cm.

Table 3- Boundary and initial conditions

3 Model Results

3.1 Thermohydraulics

Saturation, temperature, Mg concentration and vapor partial pressure profiles are shown in Figure 1. The partial pressure profile shows a descending evaporation front that divides the column in two zones: a dry zone, above, where the concentrations are high and a wet zone

below, with lower concentrations. The temperature curve displays a change in slope at the evaporation front due to the energy required for evaporation.

Figure 1 - Saturation and temperature (above), Mg concentration and vapor partial pressure (below) modeled for day 4, 8 and 12, and experimental data for day 12.

The model fits well saturation and temperature data. Mg concentration evolution is only qualitatively reproduced. Concentration beneath the evaporation front is reduced below initial values. This is due to the condensation of vapor that diffuses from the evaporation front (Figure 2). The evaporation front produces an upward vapor flux above its peak and a downward flux below it. This diffusive vapor flux is through Fick's law proportional to the gradient of vapor concentration (equivalent to vapor pressure), which depends on capillary pressure ($\left(p_g - p_{aq}\right)$, equation (7)) and on temperature through the equilibrium constant of the evaporation/condensation reaction (K_{vapour}, Table 2). A positive capillary pressure gradient gives a positive vapor flux (vapor diffuses from wet to dry), which in our experiment is upward. A positive temperature gradient gives a negative vapor flux (vapor diffuses from hot to cold), which in our experiment is downward. Above the evaporation front the low saturation and therefore low hydraulic permeability enables high capillary pressure gradients and hence an upward vapor flux (Figure 2). On the other hand, below the evaporation front the temperature gradient dominates and hence the vapor flux is downwards. The flux of liquid water is always upwards (from wet to dry) although above the evaporation front it is practically zero because the relative permeability is reduced as the saturation reduces (equation (6)).

Figure 2– Evaporation-condensation ,vapor transport and phase flow evolution. The evaporation front produces an ascent vapor flux above its peak and a descend flux below.

The saturation, concentration, temperature, energy and mass fluxes calculated here do not differ much from those calculated by Gran et al (2011b). The only notable difference is in the vapor flow; their model predicts a much bigger descending vapor flow. This might be due to the fact that, in order to represent the salts crust, they define different diffusion and thermal conductivity values for the first 1.5 cm of the domain. In our model we consider an initially homogeneous domain. Variation in porosity and saturation will induce changes in the vapor diffusion and thermal conductivity values. Still, the main difference with the model of Gran et al (2011b) lies in the geochemical computations, discussed below.

3.2 Invariant point effects on system evolution

The coexistence of epsomite-hexahydrite or hexahydrite-kieserite produces an invariant point which fixes water activity. It influences the evolution of the system, as can be noticed in Figure 3, which displays mineral mass, water activity and vapor boundary fluxes at the top. It can be seen that water activity remains constant during two intervals, a small one for the epsomite-hexahydrite invariant point (before day 4), and another for the hexahydrite-kieserite (between day 5 and 6).

Figure 3 – Mineral mass and water activity (above) and vapor fluxes (below) for the uppermost node. An invariant point produced by the coexistence of epsomite and hexahydrite occurs at day 4 and another one, associated to hexahydrite and kieserite between day 5 and 6. By fixing water activity value the invariant point controls de mass of vapor that leaves the column during these periods.

Vapor flux leaving the column also remains constant during these intervals. When the invariant points occur, mineral dehydration acts as a source term of water, releasing as much water as necessary to keep the water activity constant. As the external vapor pressure is fixed, and vapor pressure at the boundary is controlled by water activity, the vapor out-flux remains constant according to the top boundary condition described in Table 3. Therefore, during these intervals the mineral paragenesis is controlling the amount of vapor that leaves the column. The only relevant change at the top is the reduction of the more hydrated mineral fraction (epsomite), which is compensated by an increase of the less hydrated mineral (hexahidrite). The second interval is longer than the first because the passage from hexahydrite to kieserite releases more water (5 moles of water per mol of mineral) than the passage from epsomite to hexahydrite (1 mol of water per mol of mineral). Al-Jibbouri et al. (2002) and Sgualdino et al. (1987) carried out experiments which led to epsomite growth isotherms. They report a growth speed of 1.0·10-7 cm/s for a supersaturation of 0.3 g Salt/100g H_2O. This growth speed and a specific reactive surface of $2 \cdot 10^{-4}$ m^2/m^3 would give a reaction rate comparable to the vapor flux. As this reactive surface is very low, we can safely assume that these reactions occur in equilibrium.

The first mineral to precipitate is epsomite (Figure 4-a), and its precipitation front, like the evaporation front, descends through the column. The reduction in the liquid saturation increases capillary suction which reduces water activity further and produces hexahydrite precipitation. Thus, there is a second precipitation front in which epsomite is turned into

hexahydrite (Figure 4-b). As water activity reaches lower values, a third precipitation front appears in which hexahydrite is replaced by kieserite (Figure 4-d).

Figure 4 – Evolution of mineral species. The first mineral to precipitate is epsomite. As water activity diminishes epsomite is replaced by hexahydrite and finally kieserite. After an invariant occurs at the top of the column, an increase followed by a decrease in the amount of precipitated mineral occurs in the mineral front.

When an invariant point occurs at the top of the column the evaporation front remain static for a sizable time (Recall Figure 5) because the amount of mineral to be dehydrated at the column top is large. As a result, the amount of epsomite that precipitates at the mineral front increases. The positions of the mineral front when an invariant point takes place at the top of the column are highlighted in Figure 4. It can be seen that after an invariant point occurs at the top of the column the amount of precipitated epsomite increases (Figure 4-b and Figure 4-d). As the precipitation front moves downwards precipitation first decreases because water has been diluted by condensation below the evaporation front. Afterwards, an almost constant precipitation is obtained.

Figure 5 – Saturation degree and mineral mass from t=3.77 days to t=4.05 days. An invariant point occurs at the top of the column between t=3.77 and t t=3.87 days. During the invariant point occurrence epsomite precipitation increases on the mineral precipitation front and liquid saturation becomes almost constant below it.

This behavior illustrates that all processes are affected when an invariant point takes place at the top of the column. Vapor pressure at the top remains constant due to the water coming from mineral dehydration. This slows down the downwards displacement of the evaporation front. Meanwhile, the upward liquid flux keeps bringing salt to the evaporation front, which causes an increase in the amount of salt precipitated at the evaporation front. This explains the peaks of mineral mass obtained in Figure 4. This behavior was observed for different mesh sizes. Although node spacing affects these deviations values, peaks and valleys on mineral concentration remain being noticeable (for example, changing node spacing from 0.2 mm to 0.4mm produces a relative reduction in extreme values of 15%).

The accumulation of water below the evaporation front produces a sharp saturation profile (Figure 5) with an almost uniform liquid saturation below the front. This reduction in the saturation gradient decreases the liquid flow and consequently the advective and dispersive transport of solute. These processes, along with vapor condensation, reduce solutes

concentration below the evaporation front and that is why the mineral precipitation is lower than in the rest of the column.

This behavior is observed only when invariant points are occurring at the top, because this is the place where more mineral mass precipitates (note the logarithmic scale in Figure 4). The occurrence of invariant points in the rest of the column does not release enough water to affect the vapor flow because little mineral mass is available for dehydration.

4 Summary and conclusions

A laboratory experiment, in which a sand column saturated with a rich $MgSO_4$ solution was subjected to a source of heat, was modeled. The experiment involves oven dry conditions, high salinity and hydrated mineral precipitation. A reactive transport compositional formulation was adopted for the model and several coupling effects between hydrodynamic and geochemical process were considered, like sink/source of water due to evaporation-condensation, precipitation-dissolution of hydrated minerals, and capillary and osmotic effects on water activity. The code also allows representing invariant points, where mineral paragenesis prescribes water activity and therefore evaporation rate. The model was used to study the interaction of precipitation of hydrated minerals and hydrodynamics.

The model was capable of representing the occurrence of several invariant points associated to the precipitation of $MgSO_4$ hydrated minerals. Mineral precipitation-dissolution at invariant points acts as a source of water, releasing as much water as required to keep water activity constant. Model results show that the occurrence of invariant points on the top of the domain can have an appreciable effect on the outlet of vapor and on the distribution of salt precipitates along the column. In fact, invariant points could explain the spatial fluctuation on salt precipitation predicted by the model.

The experimental study of invariant points involves technical difficulties due to the unstable nature of the precipitated salts; minerals may modify its hydration content during handling or X-ray irradiation. To our knowledge this is the first time invariant points are considered in the modeling of a multiphase reactive transport experiment. The numerical model shows that the occurrence of invariant points has the potential to affect both the chemistry and hydraulics of the system, but does not have a significant impact on standard measureable variables. According to our results, the presence of peaks and valleys on mineral precipitation

distribution might evidence the influence of invariant points. This aspect that can be simply evaluated on future experiments by taking samples at different depths. These results highlight the need of more experimental evidence and should be considered in the design of future essays.

References

Acero, P. and Ayora, C. and Carrera, J. and Saaltink, M. W. and Olivella, S., 2009. Multiphase flow and reactive transport model in vadose tailings. Applied Geochemistry. 24, 1238-1250.

Al-Jibbouri, S., Strege C., Ulrich, J., 2002. Crystallization kinetics of epsomite influenced by pH-value and impurities. Journal of Crystal Growth. 236, 400–406.

Bauer, P., Held, R.J., Zimmermann, S., Linn, F., Kinzelbach, W., 2006. Coupled flow and salinity transport modelling in semi-arid environments: The Shashe River valley, Botswana. Journal of Hydrology. 316 (1–4), 163–83.

Bea S.A., Carrera, J., Ayora, C., Batlle, F. and Saaltink, M.W., 2009. CHEPROO: A fortran 90 object-oriented module to solve chemical processes in earth science models. Computers & Geosciences. 35(6), 1098–1112.

Bea, S.A., Carrera, J., Ayora, C. and Batlle, F., 2010a. Modeling of concentrated aqueous solutions: Efficient implementation of Pitzer equations in geochemical and reactive transport models. Computers & Geosciences. 36, 526–538.

Bea, S.A., Ayora, C., Carrera, J., Saaltink, M.W. and Dold, B., 2010b. Geochemical and environmental controls on the genesis of soluble efflorescent salts in Coastal Mine Tailings Deposits: A discussion based on reactive transport modeling. Journal of Contaminant Hydrology. 111, 65-82.

Bechtold, M., Vanderborght, J., Weihermüller, L., Herbst, M., Günther, T., Ippisch, O., Kasteel, R., Vereecken, H., 2011. Upward Transport in a Three-Dimensional Heterogeneous Laboratory Soil under Evaporation Conditions. Vadose Zone Journal. 11(2)., doi: 10.2136/vzj2011.0066.

Cortes-Jimenez, J.M., Troyo-Dieguez, E., Murillo-Amador, B., Garcia-Hernandez, J.L., Garatuza-Payan, J., Lee, S.S., 2007. Diagnosing and modeling water quality parameters of the Yaqui valley's aquifer in northwest Mexico for salinity risk evaluation. Fresenius Environmental Bulletin. 16(5), 517–523.

Dao, V.N.T., Morris P.H., Dux P.F., 2008. On equations for the total suction and its matric and osmotic components. Cement and Concrete Research. 38, 1302–1305

Ebigbo, A., Bielinski, A., Kopp, A., Class, H. and Helmig, R., 2006. Numerical Modeling of CO2 Sequestration with MUFTE-UG. CMWR XVI - Computational Methods in Water Resources, XVI International Conference, Copenhagen, Denmark (http://dx.doi.org/10.4122/1.1000000690).

Fayer, M.J., Gee, G.W. and Jones, T.L., 1986. UNSAT-H Version 1.0: Unsaturated flow code documentation and application for the Hanford Site. Report Number PNL-5899, Pacific Northwest Laboratory, Richland, Washington.

Fayer, M. J. and Simmons, C. S., 1995. Modified Soil-Water Retention Functions For All Matric Suctions. Water Resources Research. 31, 1233–1238.

Gamazo, P., Bea, S.A., Saaltink, M.W., Carrera, J. and Ayora, C., 2011. Modeling the interaction between evaporation and chemical composition in a natural saline system. Journal of Hydrology. 401, 154-164.

Gamazo, P., Saaltink, M.W., Carrera, J., Slooten, L. and Bea, S.A., 2012. A consistent compositional formulation for multiphase reactive transport where chemistry affects hydrodynamics. Advances in Water Resources. 35, 83-93.

Garcia-Guinea J., Abella R., Sanchez-Moral S., Benito R., and Martin-Ramos D., 2000. Examining hydrated minerals using optically stimulated X-ray diffraction, an inexpensive modification of traditional diffractometers. Journal of Sedimentary Research. 70 (4), 964-967

Ghassemi, F., Jakeman, A.J., Nix, H.A., 1991. Human induced salinization and the use of quantitative methods. Environment International. 17 (6), 581-594.

Gran, M., Carrera, J., Massana, J., Saaltink, M.W., Olivella, S., Ayora, C. and Lloret, A., 2011a. Dynamics of water vapor flux and water separation processes during evaporation from a salty dry soil. Journal of Hydrology. 396, 215-220.

Gran, M., Carrera, J., Olivella, S., and Saaltink, M. W., 2011b. Modeling evaporation processes in a saline soil from saturation to oven dry conditions. Hydrology and Earth System Sciences. 15, 2077-2089

Guglielmini, L., Gontcharov, A., Aldykiewicz A.J., Stone, H.A., 2008. Drying of salt solutions in porous materials: Intermediate-time dynamics and efflorescence. Physics Of Fluids. 20, 077101.

Grevel, K. D. and Majzlan, J., 2009. Internally consistent thermodynamic data for magnesium sulfate hydrates. Geochimica et Cosmochimica Acta. 73, 6805-6815.

Harvie, C. H., Moller, N., & Weare, H. 1984. The prediction of mineral solubilities in natural waters: The Na-K-Mg-Ca-H-Cl-SO_4-OH-HCO_3-CO_3-CO_2-H_2O system to high ionic strengths at 25°C. Geochimica et Cosmochimica Acta. 48, 723-75 1.

Kwak, H.T., Zhang, G. and Chen, S., 2005. The effects of salt type and salinity on formation water viscosity and NMR Responses. International Symposium of the Society of Core Analysts (Toronto, Canada 21-25, August 2005). SCA2005-51.

Lefebvre, R., Hockley, D., Smolensky, J., Lamontagnec, A., 2001. Multiphase transfer processes in waste rock piles producing acid mine drainage: 2. Applications of numerical simulation. Journal of Contaminant Hydrology. 52(1–4), 165–186

Lide, D. R., 2000. CRC Handbook of Chemistry and Physics, 81st ed. CRC Press, Boca Raton, Fla., London.

Massana, J., 2005. Influència de la salinitat en el flux multifàsic en solumnes de sòl obertes i sota condicions d'evaporació. Master thesis, Technical University of Catalonia (UPC).

Mayer, K.U., S. G. Benner, and D. W. Blowes, 2006. Process-based reactive transport modeling of a permeable reactive barrier for the treatment of mine drainage. Journal of Contaminant Hydrology. 85, 195-211

Milly, P. C. D., Thesis (M.S.), 1980. The coupled transport of water and heat in a vertical soil column under atmospheric excitation. Massachusetts Institute of Technology, Dept. of Civil Engineering.

Mills, R., Lu, C., Lichtner, P.C. and Hammond, G., 2007. Simulating Subsurface Flow and Transport on Ultrascale Computers using PFLOTRAN. Journal of Physics Conference Series. 78, 012051, doi:10.1088/1742-6596/78/1/012051.

Molins, S. and Mayer, K. U., 2007. Coupling between geochemical reactions and multicomponent gas and solute transport in unsaturated media: A reactive transport modeling study. Water Resources Research. 43(5), W05435 , doi:10.1029/2006WR005206.

Nachshon, U., Weisbrod,N., Dragila, M.I. and Grader, A., 2011. Combined evaporation and salt precipitation in homogeneous and heterogeneous porous media. Water Resources Research. 47, W03513, doi:10.1029/2010WR009677.

Nassar, I. N. and Horton, R., 1989. Water Transport in Unsaturated Non-Isothermal Salty Soil. 2. Theoretical Development. Soil Science Society of America Journal. 53, 1330–1337.

Palandri, J.,L. and Kharaka, Y., K., 2004. A compilation of rate parameters of water-mineral interaction kinetics for application to geochemical modeling. U.S. Geological Survey, Open file report, 2004-1068, National Energy Technology Laboratory – United States Department of Energy, Menlo Park, California

Parkhurst, DL, Appelo, CAJ. 1999. User's guide to PHREEQC (version 2): A computer program for speciation, batch-reaction, one-dimensional transport, and inverse geochemical calculations (http://wwwbrr.cr.usgs.gov/projects/GWC_coupled/phreeqc/html/final.html).

Pitzer, S., 1973. Thermodynamics of electrolytes. I. Theoretical basis and general equations. Journal of Physical Chemistry. 77(2), 268–277.

Qadir, M., Ghafoor, A., Murtaza, G., 2000. Amelioration strategies for saline soils: A review. Land Degradation & Development. 11(6), 501–21.

Rad, M.N., and Shokri N., 2012. Nonlinear effects of salt concentrations on evaporation from porous media. Geophysical Research Letters. 39, L04403, doi:10.1029/2011GL050763.

Risacher, F. and Clement, A., 2001. A computer program for the simulation of evaporation of natural waters to high concentration. Computers & Geosciences. 27(2), 191–201.

Remson, I., Hornberger G. M., Molz F. J., 1971. Numerical Methods in Subsurface Hydrology. Wiley-Interscience, New York.

Saaltink, M. W., Ayora, C., and Carrera, J., 1998. A mathematical formulation for reactive transport that eliminates mineral concentrations. Water Resources Research. 34(7), 1649–1656.

Saaltink, M.W., Batlle, F., Ayora, C., Carrera, J. and Olivella, S., 2004. Retraso, a code for modeling reactive transport in saturated and unsaturated porous media. Geologica Acta. 2(3), 235–251.

Silva, O., and Grifoll, J., 2007. A soil-water retention function that includes the hyper-dry region through the BET adsorption isotherm. Water Resources Research. 43, W11420, doi:10.1029/2006WR005325.

Sgualdino, G., Vaccari, G., Aquilano, D. and Rubbo, M., 1987. Growth kinetics of epsomite (MgSo4. 7H2O). Journal of crystal growth. 83, 523-527.

Slooten, L.J., Batlle, F., and Carrera, J., 2010. An XML based Problem Solving Environment for Hydrological Problems. XVIII Conference on Computational Methods in Water Resources CMWR (http://congress.cimne.com/cmwr2010).

Steefel, C. I.; DePaolo, D. J. & Lichtner, P. C. , 2005. Reactive transport modeling: An essential tool and a new research approach for the Earth sciences. Earth and Planetary Science Letters. 240, 539-558.

Wang, A., Freeman, J. J. and Jolliff, B. L., 2009. Phase transition pathways of the hydrates of magnesium sulfate in the temperature range 50°C to 5°C: Implication for sulfates on Mars. Journal of Geophysical Research. 114 , E04010, doi:10.1029/2008JE003266.

Wenninger, J., Beza, D.T., Uhlenbrook, S., 2010. Experimental investigations of water fluxes within the soil–vegetation–atmosphere system: Stable isotope mass-balance approach to partition evaporation and transpiration. Physics and Chemistry of the Earth, Parts A/B/C. 35(13–14), 565–570.

Wissmeier, L., Barry, D.A., 2008. Reactive transport in unsaturated soil: Comprehensive modelling of the dynamic spatial and temporal mass balance of water and chemical components. Advances in Water Resources. 31(5), 858–875.

Xu, T. and Pruess, K., 1998. Coupled modeling of non-isothermal multiphase flow, solute transport and reactive chemistry in porous and fractured media: 1. Model development and validation. Lawrence Berkeley National Laboratory Report LBNL-42050, Berkeley, California.

Xu, P., Shao, Y.P., 2002. A salt-transport model within a land-surface scheme for studies of salinisation in irrigated areas. Environmental Modelling & Software. 17(1), 39–49.

Zee, S. E. A. T. M. van der, 1990. Transport of reactive solutes in spatially variable unsaturated soils, in: Roth, K., Flühler, H., Jury, W.A., Parker, J.C. (Eds.), Field-scale solute and water transport through soil. Workshop Ascona Proceedings, Birkhäuser, Basel pp 269-279.

Nomenclature

a_i	Activity of species i
aq	Sub index for the aqueous phase
c_i	Moles of the species i
$\mathbf{c}_{aq}$	Vector of the concentration of aqueous species
$\mathbf{c}_{gas}$	Vector of the concentration of gaseous species
$\mathbf{c}_{imm}$	Vector of the concentration of immobile species
d_l	Longitudinal dispersion coefficient
$\mathbf{D}_\alpha^{diff}$	Diffusion coefficient of phase α
$\mathbf{D}_\alpha^{disp}$	Dispersion coefficient for phase α $\mathbf{D}_\alpha^{disp} = d_l \lvert \mathbf{q}_\alpha \rvert \mathbf{I}$
$e_{i,\alpha}$	Molar internal energy of the specie i in phase α.
E_α	Volumetric internal energy of phase
f_{cap}	Correction factor for water activity due to capillary effects
f_E	Energy sink-source term.
$\mathbf{f}$	Vector of source-sink terms
$\mathbf{f}'$	External component source-sink term $\mathbf{f}' = \mathbf{U} \cdot \mathbf{f}$
g	Sub index for the gaseous phase
$\mathbf{g}$	Gravity vector
i	Sub index indicating a species
$\mathbf{i}_c$	Conductive heat flux
$\mathbf{i}_{E,\alpha}$	heat flux due to the motion of phase α
$\mathbf{j}_{D_\alpha,i}$	Diffusive-dispersive flux of component i in phase α calculated by Fick's law: $\mathbf{j}_{D_\alpha,i} = -\left(\mathbf{D}_\alpha^{diff}\phi\theta_\alpha\tau + \mathbf{D}^{disp}\right)\cdot \nabla\left(u_{i,\alpha}\right)$
k_c^T	Thermal conductivity of the medium
$k_{r,\alpha}$	Relative permeability for phase α
K_j	Equilibrium constant of reaction j
$\mathbf{K}$	Intrinsic permeability
$L_\alpha\left(u_{i,\alpha}\right)$	Transport operator, null for immobile phases, for mobile phases: $L_\alpha\left(u_{i,\alpha}\right) = -\nabla\cdot\left(u_{i,\alpha}\mathbf{q}_\alpha\right) - \nabla\cdot\left(\mathbf{j}_{D_\alpha,i}\right)$
$\mathbf{L}(\ )$	Vector of transport operators
M_i	Molecular weight of species i
p_i	Partial pressure of gaseous species i
p_α	Pressure of phase α
$\mathbf{q}_\alpha$	Flow of phase α, calculated by Darcy's law: $\mathbf{q}_\alpha = -\frac{\mathbf{K}k_{r,\alpha}}{\mu_\alpha}\left(\nabla p_\alpha - \rho_\alpha \mathbf{g}\right)$
R	Universal gas constant
S_α	Saturation of α phase
T	temperature
$u_{i,\alpha}$	Concentration of component i in α phase
$\mathbf{u}_{aq}$	Vector of aqueous component
$\mathbf{u}_g$	Vector of gaseous component
$\mathbf{u}_{imm}$	Vector of immobile components
$\mathbf{U}$	Component matrix
α	Sub index indicating a phase
θ_α	Volumetric fraction of phase α
μ_α	Viscosity of phase α
ρ_α	Density of phase α
τ	Tortuosity factor
ϕ	Porosity

Table 1

Table 1 - Constitutive equations

Retention curve (modified van Genuchten model)	$S_{aq} = S_i + (1 - S_i) S_e$ $S_e = \left(1 + \left(\left(P_g - P_{aq}\right)/P_0\right)^{\frac{1}{1-\lambda}}\right)^{-\lambda}$ $S_i = S_{\min}^0 \beta \ln\left(P_c^{dry} / \left(P_g - P_{aq}\right)\right)$	$P_0 = 25\text{x}10^{-4}\,[\text{MPa}]$ $\lambda = 0.93\,;\ \beta = 0.1$ $S_{\min}^0 = 0.08$ $P_c^{dry} = 650[\text{MPa}]$
Relative permeability	$K_{r,aq} = \begin{cases} K_{r,aq}^0 & S_{aq} > S_{aq,min} \\ K_{r,aq}^0 \left(S_{aq}/S_{aq,min}\right)^{\gamma} & S_{aq} < S_{aq,min} \end{cases}$ $K_{r,aq}^0 = \sqrt{S_e^{'}\left(1 - \left(1 - S_e^{'1/\lambda}\right)^{\lambda}\right)^2}$ $K_{r,g} = 1 - K_{r,aq}$	$S_e^{'} = \dfrac{S_{aq} - S_{\min}^0}{1 - S_{\min}^0}$ $S_{aq,min} = 0.1$ $\gamma = 5$
Intrinsic permeability	$\mathbf{K} = \mathbf{K}_0 \left(\dfrac{\phi}{\phi_0}\right)^3 \left(\dfrac{1-\phi_0}{1-\phi}\right)^2$	$\mathbf{K}_0 = 2.8\text{x}10^{-11}\left[m^2\right]$ $\phi_0 = 0.4$ Initial (nonreactive) porosity
Porosity	$\phi = \phi_0 + \sum_{i=1}^{Nms} c_i \cdot V_{m,i}$	c_i concentration of mineral specie i $V_{m,i}$ molecular volume of mineral specie i
Phase density	$\rho_{aq} = P_0 \exp\left(\alpha_\rho T + \beta\left(P_{aq} - P_0\right) + \gamma_\rho \left(\sum_{i \neq h_2 o} \omega_l^i\right)\right)$ $\rho_g = \dfrac{p_{vap} \cdot M_{vap} + p_{air} \cdot M_{air}}{R\left(T + 273.15\right)}$	$P_0 = 1002.6[\text{MPa}]$ $\alpha_\rho = -3.4\text{x}10^{-4}\left[{}^{\text{o}}C^{-1}\right]$ $\beta = 4.5\text{x}10^{-4}\left[\text{MPa}^{-1}\right]$ $\gamma_\rho = 0.6923$ $M_{vap} = 0.018[Kg/mol]$ $M_{air} = 0.02895[Kg/mol]$
Phase viscosity	$\mu_{\text{liq}} = 2.1\text{x}10^{-12} \cdot \exp\left(\dfrac{1808.5}{T + 273.15}\right)[\text{MPa} \cdot \text{s}]$ $\mu_{\text{gas}} = 1.48\text{x}10^{-12} \cdot \exp\left(\dfrac{119.4}{T + 273.15}\right)[\text{MPa} \cdot \text{s}]$	
Phase diffusion	$D_g^{diff} = 5.9x10^{-6}\left(\dfrac{\left(T + 273.15\right)^{2.3}}{P_g}\right)\left[m^2/s\right]$ $D_{aq}^{diff} = 1.1x10^{-4} \exp\left(\dfrac{-24539}{R \cdot \left(T + 273.15\right)}\right)\left[m^2/s\right]$	
Phase dispersion	$\mathbf{D}_\alpha^{disp} = d_l \lvert \mathbf{q}_\alpha \rvert \mathbf{I}$	$d_l = 0.015m$
Vapor diffusion enhancement	$\theta_{gas} \tau = 1$	
Thermal conductivity	$\lambda = \lambda_{sat}^{S_l} \lambda_{dry}^{(1-S_l)}\left[\text{Wm/K}\right]$	$\lambda_{sat} = 1.44\,;\ \lambda_{dry} = 1.54$

Table 2 – Chemical reactions considered

$H_2O_{(l)} \Leftrightarrow H_2O_{(g)}$	$K_{vapour} = 1.36075\text{x}10^{11} \exp\left(\frac{-5239.7}{273.15+T}\right)\left[\frac{\text{Pa}\cdot Kgh_2o}{mol}\right]$
$air_{(l)} \Leftrightarrow air_{(g)}$	$K_{air} = 2.9\text{x}10^{8}\left[\frac{\text{Pa}\cdot Kgh_2o}{mol}\right]$
$H_2O_{(l)} \Leftrightarrow H^+ + OH^-$	$K_{oh} = 10^{-14}$
$Mg^{2+} + OH^- \Leftrightarrow Mg(OH)^+$	$K_{mg(oh)} = 10^{2.19}$
$SO_4^{2+} + H^+ \Leftrightarrow H(SO_4)^-$	$K_{h(so4)} = 10^{1.98}$
$Mg^{2+} + SO_4^{2-} + 7H_2O_{(l)} \Leftrightarrow epsomite$	$K_{epsomite} = 10^{1.8881}$
$Mg^{2+} + SO_4^{2-} + 6H_2O_{(l)} \Leftrightarrow hexahydrite$	$K_{hexahydrite} = 10^{1.7268}$
$Mg^{2+} + SO_4^{2-} + 5H_2O_{(l)} \Leftrightarrow pentahydrite$	$K_{pentahydrite} = 10^{1.285}$
$Mg^{2+} + SO_4^{2-} + 4H_2O_{(l)} \Leftrightarrow leonhardite$	$K_{leonhardite} = 10^{0.887}$
$Mg^{2+} + SO_4^{2-} + H_2O_{(l)} \Leftrightarrow kieserite$	$K_{kieserite} = 10^{0.123}$

Table 3- Boundary and initial conditions

Initial conditions	$S_{aq}=1;\ T=25^{o}C;$	
	Hydrostatic liquid pressure: $P_{aq}^{top}=101325[\mathrm{Pa}]$	
Top boundary gas flow	$j_i^{top}=\alpha_j\left(P_g^{ext}-P_g^{top}\right)\cdot c_i^{*}+\beta_j\left(P_i^{ext}-P_i^{top}\right)$	$\alpha_j=43\left[m/\left(\mathrm{MPa}\cdot s\right)\right]$
		$\beta_j=1.5\left[mol/\left(\mathrm{MPa}\cdot s\cdot m^2\right)\right]$
	$c_i^{*}=\begin{cases}c_i^{ext} & P_g^{ext}>P_g^{top}\\ c_i^{top} & P_g^{ext}<P_g^{top}\end{cases}$	$P_{h_2o}^{ext}=3172[\mathrm{Pa}]$
		$P_{air}^{ext}=98152[\mathrm{Pa}]$
Top boundary heat flow	$j_{e,in}=750[J/s]$	
Heat loss	$j_{e,lose}=\alpha_T\left(T_{ext}-T\right)$	$\alpha_T=25\left[J/\left(K\cdot s\right)\right];\ T_{ext}=26[^{o}C]$
Initial concentrations	$H_2O_{(aq)}=5.551\mathrm{x}10^{1}[m]$	$Cl^{-}=4.00\mathrm{x}10^{-3}[m]$
	$air_{(aq)}=5.453\mathrm{x}10^{-4}[m]$	$H_2O_{(g)}=3.173\mathrm{x}10^{-3}[\mathrm{MPa}]$
	$Mg^{2+}=5.88\mathrm{x}10^{-2}[m]$	$air_{(g)}=9.815\mathrm{x}10^{-2}[\mathrm{MPa}]$
	$SO_4^{2-}=5.68\mathrm{x}10^{-2}[m]$	$\phi=0.4$

Figure 1

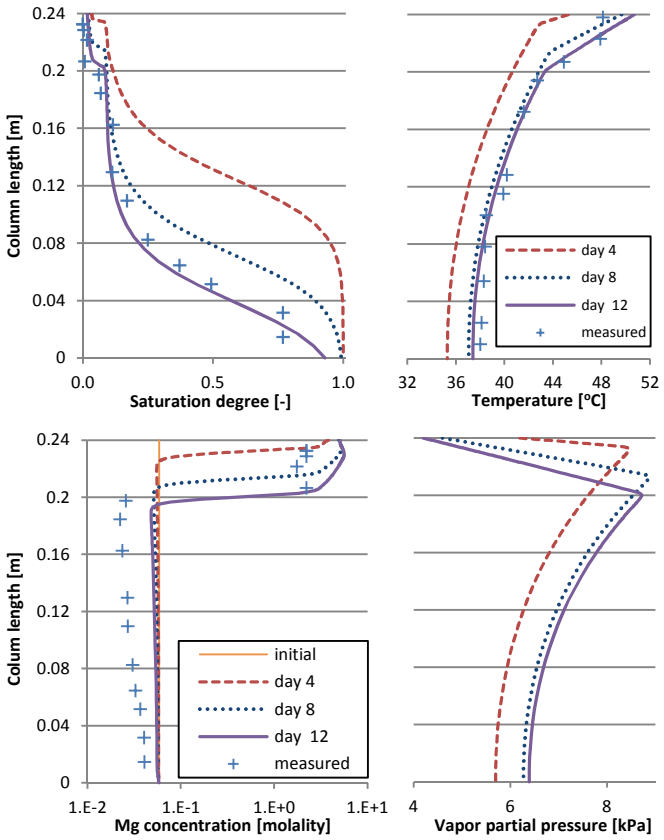

Figure 2

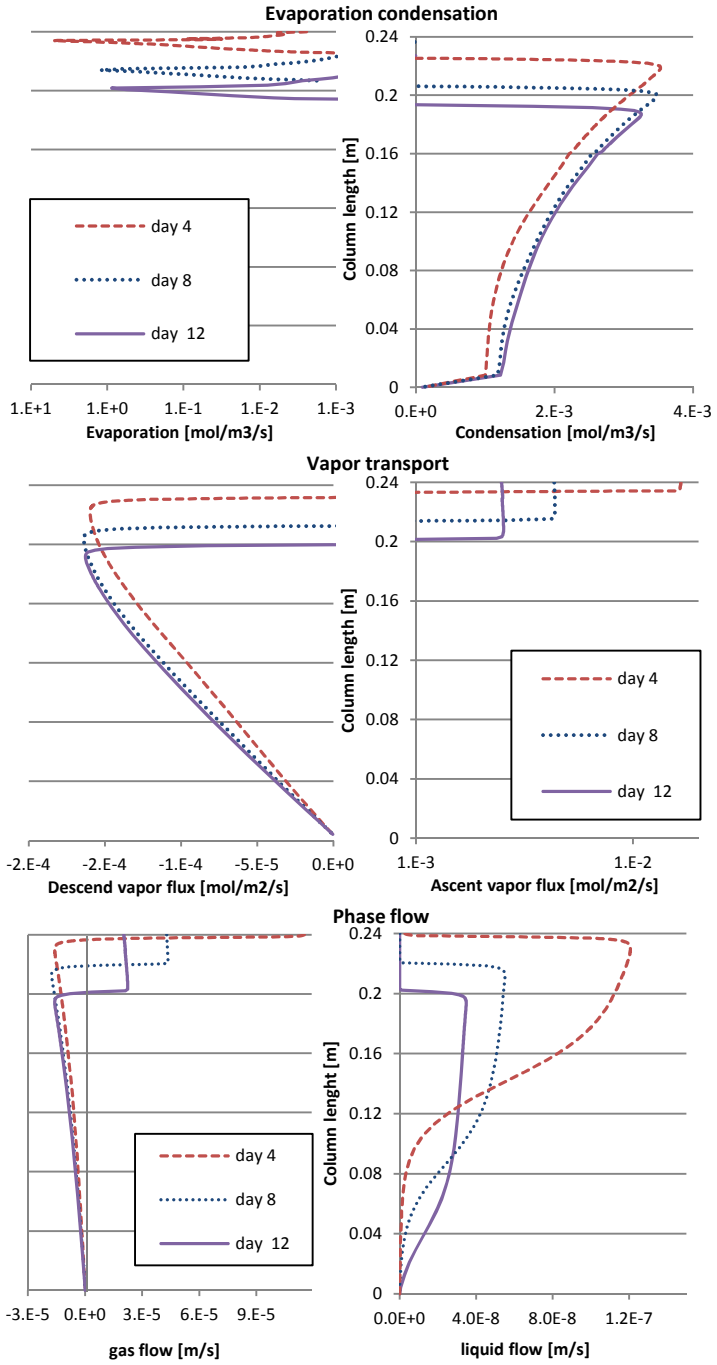

Figure 3

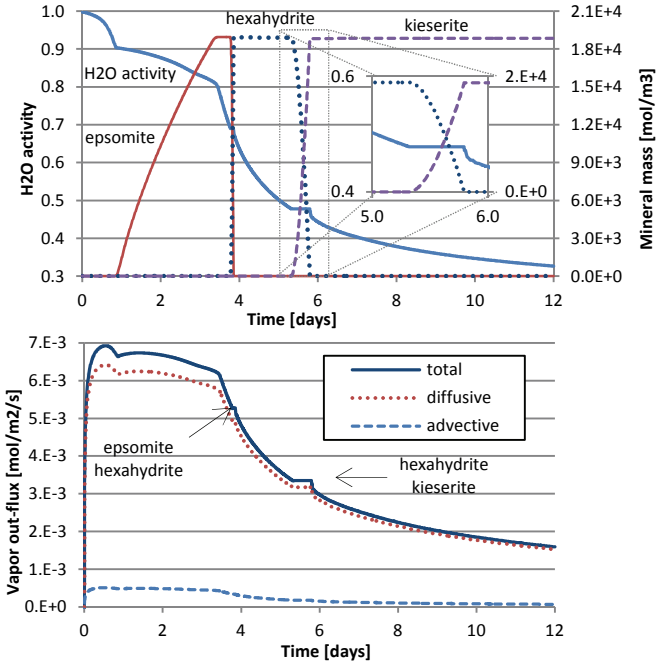

Figure 4

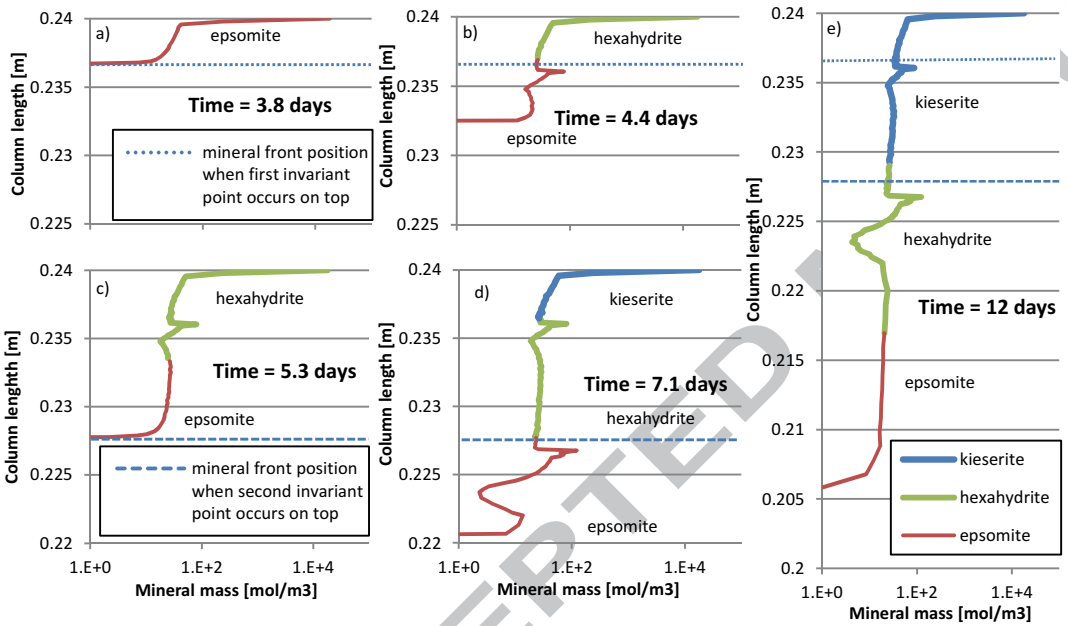

Figure 5